Modeling and Simulation of Hydrogen Energy Storage System for Power-to-gas and Gas-to-power Systems

Jianlin Li, Guanghui Li, Suliang Ma, Zhonghao Liang, Yaxin Li, and Wei Zeng

***Abstract*—By collecting and organizing historical data and typical model characteristics, hydrogen energy storage system (HESS)-based power-to-gas (P2G) and gas-to-power systems are developed using Simulink. The energy transfer mechanisms and numerical modeling methods of the proposed systems are studied in detail. The proposed integrated HESS model covers the following system components: alkaline electrolyzer (AE), high-pressure hydrogen storage tank with compressor (CM & H_2 tank), and proton-exchange membrane fuel cell (PEMFC) stack. The unit models in the HESS are established based on typical *U-I* curves and equivalent circuit models, which are used to analyze the operating characteristics and charging/discharging behaviors of a typical AE, an ideal CM & H_2 tank, and a PEMFC stack. The validities of these models are simulated and verified in the MicroGrid system, which is equipped with a wind power generation system, a photovoltaic power generation system, and an auxiliary battery energy storage system (BESS) unit. Simulation results in MATLAB/Simulink show that electrolyzer stack, fuel cell stack and system integration model can operate in different cases. By testing the simulation results of the HESS under different working conditions, the hydrogen production flow, stack voltage, state of charge (SOC) of the BESS, state of hydrogen pressure (SOHP) of the HESS, and HESS energy flow paths are analyzed. The simulation results are consistent with expectations, showing that the integrated HESS model can effectively absorb wind and photovoltaic power. As the wind and photovoltaic power generations increase, the HESS current increases, thereby increasing the amount of hydrogen production to absorb the surplus power. The results show that the HESS responds faster than the traditional BESS in the microgrid, providing a solid theoretical foundation for later wind-photovoltaic-HESS-BESS integration.**

***Index Terms*—Hydrogen energy storage system (HESS), green electricity hydrogen production, compressor, hydrogen storage tank, proton-exchange membrane fuel cell (PEMFC), wind-photovoltaic-HESS-BESS integration.**

I. Introduction

In the context of "carbon emission peak & carbon neutrality" strategies, the construction of a new power system with renewable energy as the mainstay has become a general trend. According to the National Energy Administration of China, by the end of 2020, the national installed capacity of renewable energy power generation had reached 934 GW, which was a year-on-year increase of approximately 17.5%. However, owing to the fluctuations and intermittencies of renewable energy as well as the limitations of transmission lines, the phenomenon of wind and photovoltaic (PV) abandonment is becoming increasingly serious and cannot adapt to real-time changing load demands on the customer side [1]. As a green and zero-carbon energy type with abundant reserves, high calorific value, high energy density, and diverse sources, hydrogen energy is regarded as the "ultimate energy" and is an excellent energy storage medium in the 21st century [2]. Global "green hydrogen" production costs have decreased by 40% over the last five years. At present, the cost of hydrogen production from renewable energy in China is 2.05 ¥/Nm^3, the energy consumption is 5 kWh/($N \cdot m^3$), the electrolysis efficiency is 60%-75%, and the hydrogen fuel-cell efficiency is 50%. Therefore, it is crucial to improve the key technologies of "green hydrogen" production, storage, and transportation as well as fuel-cell control strategies.

As a new type of zero-carbon energy storage, the hydrogen energy storage system (HESS) using hydrogen as the medium has gradually achieved superiority in terms of environmental benefits, operational stability, and smoothed renewable energy fluctuations in systems such as microgrids (MGs) and the regional energy internet. In the MG system, the surplus electricity from renewable power sources (such as wind power and PVs) is converted to hydrogen by the electrolysis of water, and the hydrogen is stored in a tank for future use to realize medium- and long-term energy storage. Hydrogen can then be transported to a hydrogen refueling station through the hydrogen supply chain, or can be grid-connected by hydrogen fuel-cell power generation to maximize the utilization of hydrogen energy. The HESS in an MG can enable synergistic effects among the different distributed power sources, which can effectively improve the flexibilities of the distributed power sources in the MG, re-

Manuscript received: November 1, 2021; revised: March 8, 2022; accepted: May 28, 2021. Date of CrossCheck: May 28, 2021. Date of online publication: July 11, 2022.

This work was supported by the State Grid Jiangxi Electric Power Co., Ltd. (No. 52182020008K) and Beijing Millions of Talents Funding Project (No. 2020A30).

J. Li, G. Li (corresponding author), S. Ma, Z. Liang, and Y. Li are with the School of Electrical and Control Engineering, North China University of Technology, Beijing 100144, China (e-mail: dkyljl@163.com; lgh@mail.ncut.edu.cn; msl13811581885@ncut.edu.cn; tgncut@126.com; lyxTGY@126.com).

W. Zeng is with the State Grid Jiangxi Electric Power Co., Ltd. Electric Power Research Institute, Nanchang 330096, China (e-mail: KevinL2021@126.com).

DOI: 10.35833/MPCE.2021.000705

duce the rates of abandonment of wind and PV powers, and smooth the fluctuations of power generation systems such as wind and PV power systems [3], [4]. Therefore, comprehensive utilization of renewable energy systems equipped with a HESS has become a key technology to smooth the fluctuations of wind and PV powers in the MG to fully utilize distributed sources and improve the stability of MG operation. The mathematical modeling and dynamic simulation studies of HESS integration are crucial for later development of smart grids; they are also important for the construction of new power systems with new energy sources as the mainstay. Establishing an accurate HESS integration model for observing the operational characteristics of HESS, including the steady-state characteristics and dynamic performance, can provide a solid foundation for research and demonstration of a comprehensive hydrogen energy utilization system in an MG.

In recent years, large numbers of studies have been devoted to the modeling and control strategies of wind-PV-HESS-battery energy storage system (BESS) hybrid systems such as modeling technologies of wind power hydrogen production, PV-coupled hydrogen production, and other renewable-energy-coupled hydrogen production system as well as analyses of the economic benefits of renewable energy hydrogen production systems [5]-[8]. Reference [9] designed a hybrid PV-hydrogen production system based on intelligent control, and developed an adaptive fuzzy-logic control (FLC) unit to control the inverter, which was optimized by a genetic algorithm to greatly improve the grid-connected characteristics of the hybrid PV-hydrogen production system. Reference [10] proposed a new proton-exchange membrane fuel cell (PEMFC) modeling method that used data-driven modeling and the datasheet provided by the equipment manufacturer; the data were used to construct the model without the need for experimental testing of the real stack. The simulation results were close to the expected results, and the errors were within ±1%, which is helpful for promoting the development of fuel-cell power systems [10]. Reference [3] proposed a modeling and control strategy for wind-PV hybrid hydrogen production and energy storage system; their model supported different topology choices and realized a capacity-optimized configuration of the distributed power generating units and HESSs. Reference [11] compared the dynamic equivalent circuit models of various fuel cells and built a passive model based on the experimental data of a 25 W PEMFC, which can realize automatic responses to external excitations of the fuel-cell stack; however, this work did not present experimental tests on the compared models and only analyzed the characteristics of different models. Reference [12] developed a proton-exchange membrane electrolyzer model based on Simulink; the changes in stack efficiency, voltage loss, and losses of other components such as the cathode and anode, were considered in the model. The dynamic changes during operation of the proton-exchange membrane electrolyzers were tested to prove that the proposed model was consistent with data from experiments. The above studies focused on system models such as renewable energy hydrogen production and hydrogen fuel-cell power generation systems. However, they did not model the entire process of hydrogen production, storage, and application, or consider the impact of separate hydrogen sales on the system.

There are many reported studies on integrated HESS modeling and coupling of renewable systems with HESSs [13]-[15]. The combination of HESS and wind turbines was found to be an economical risk quantification model for participating in the electricity market in China [16]. Some scholars have used the surrogate modeling method to construct and analyze HESSs in recent years, but their efforts were mainly on optimization of the equipment structure and did not consider the HESS integration with the power system [17]. A four-layer construction framework for a digital twin of an alkaline electrolyzer (AE) was reported in [18]; based on multidimensional data obtained from the physical layer and combined with the working mechanism of the AE, a digital twin of the electrolyzer was constructed via hybrid modeling to integrate the theoretical and data-driven models, which implemented virtual mapping of the physical AE. Reference [19] presented the modeling of an autonomous system powered by a PV generator and fuel-cell stack, including a PV array, an AE, a high-pressure hydrogen storage tank with compressor (CM & H_2 tank), and fuel-cell stack. The hydrogen produced by the electrolyzer can be retained as compressed gaseous storage. The modeling of such a storage type is based on the ideal gas law, with the aim of determining the hydrogen pressure. The research in this paper also provides a reference for further study of hydrogen conversion systems coupled with renewable energy systems. A comprehensive PEMFC simulation model was established in [20], where an intelligent method was proposed for identifying the voltage and temperature of a PEMFC system. The proposed model was experimentally verified to exhibit good dynamic response characteristics.

Therefore, a basic integrated HESS model has been introduced using Simulink in the present study. The system components include the AE, CM & H_2 tank, and PEMFC, modeled by analyzing the charging/discharging behaviors and energy transfer mechanism of the system using numerical modeling methods. Finally, the model established in this paper is validated using an MG simulation system containing wind power, PVs, and BESS. The simulation results confirm and demonstrate the applicability of the proposed integrated HESS model to the MG. By observing the simulation results under different working conditions, the relationships between the parameters such as hydrogen production flow rate, stack voltage, state of hydrogen pressure (SOHP), and power generation curve of the HESS, are analyzed. The simulation results effectively reflect the typical operating characteristics of AEs, CM & H_2 tanks, and PEMFCs in HESSs. The simulation results also show that the proposed model can effectively represent the energy transfer mechanism of the coupled HESS system, which is expected to provide a theoretical basis for large-scale application of renewable-energy-coupled HESSs in the future.

II. Description of Grid-connected Wind-PV-HESS-BESS Hybrid Systems

Figure 1 shows a simplified schematic of the grid-connected wind-PV-HESS-BESS hybrid systems used to develop the integrated HESS model. It mainly consists of three parts: renewable energy sources and auxiliary ESS, the HESS, and the power grid. The HESS includes an AE, a power conversion system (PCS) unit, a CM & H_2 tank, and a PEMFC. The interconnection of the distributed power sources and electrolyzers in the power grid is realized through the PCS. When there is a surplus of renewable energy such as wind and PV, the surplus electricity in the MG is sent to an AE to produce hydrogen, which is then compressed and stored in a high-pressure storage tank. The stored hydrogen is sent to the fuel cell to generate electricity or to the hydrogen refueling station of the downstream industrial chain through the supply chain. Through this, the full lifecycle application of hydrogen in HESS can be realized [21], [22]. To avoid shortage of hydrogen supply during shortage of renewable energy, the wind power and PV power are combined with grid-assisted power to produce hydrogen.

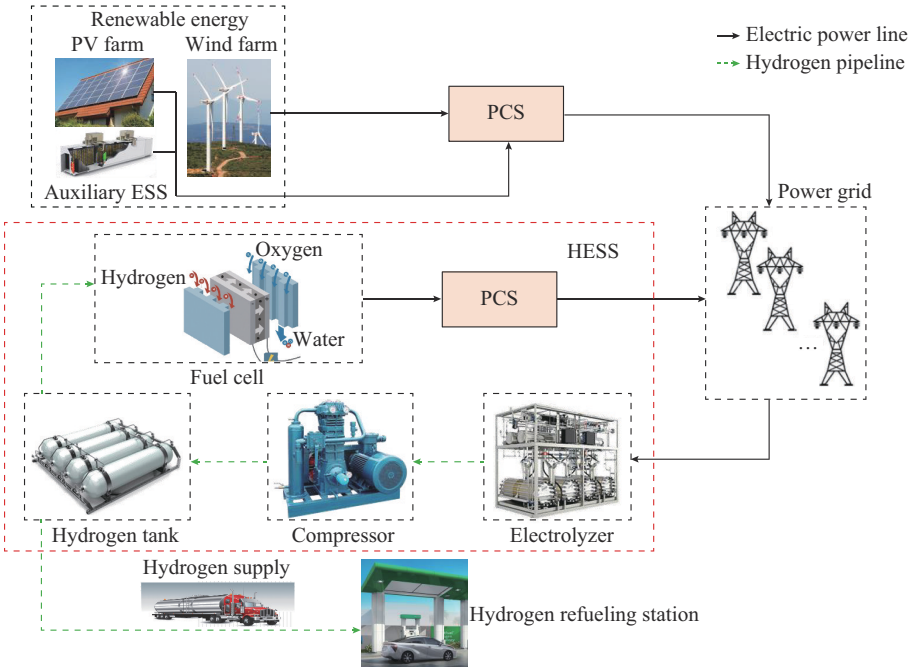

Fig. 1. Simplified schematic of grid-connected wind-PV-HESS-BESS hybrid systems used to develop integrated HESS model.

This MG system, where the grid parameters are 380 V/50 Hz, mainly comprises distributed power supply, load, BESS devices, and HESS. The distributed energy sources include wind power system, PVs, BESSs, and HESSs. The wind power system, PVs, AC load, and HESS are all connected to the grid through the AC busbar. Auxiliary BESS devices are installed in the wind and PV power generation systems. To ensure the stability of the AC bus, it is necessary to distribute the power of the HESS and BESS reasonably. Therefore, the power distribution principle of this MG system includes the following two cases.

1) Case 1: when there is excess differential power in the MG (i. e., the distributed power supply is greater than the load power to meet the load power demand), there are two energy flow paths, namely hydrogen production by electrolysis and BESS charging. When the state of charge (SOC) of the BESS is high, the electrolytic hydrogen production power allocation ratio is higher, and more power is used for hydrogen production to slow the increase of SOC. When the SOC of the BESS is low, the distribution power of electrolytic hydrogen production is lower, which is used to mainly boost the SOC of the BESS and prevent the BESS from being in the deep discharging area for a long time. When the SOC of the BESS is within a reasonable working range, the allocated power depends mainly on the SOHP of the hydrogen tank. When the SOHP is low, the electrolytic hydrogen production absorbs more power to boost the SOHP. When the SOHP is high, electrolytic hydrogen production absorbs less power, thus preventing the SOHP from being too high.

2) Case 2: when the differential power within the MG is insufficient, there are two power flow paths, namely PEMFC and BESS discharging. When the SOC of the BESS is high, the power allocated by the PEMFC is low; therefore, the priority is to discharge from the BESS to reduce its SOC and prevent the BESS from being in the deep charging area for a long time. When the SOC of the BESS is low, high power is allocated by the PEMFC, and power is preferentially supplied by the PEMFC to prevent the SOC of the BESS from decreasing. When the SOC of the BESS is within a reasonable working range, the allocated power mainly depends on the SOHP of the HESS. When the SOHP is low, the PEMFC releases less power to avoid continuous decrease of the SOHP. When the SOHP is high, the PEMFC releases more power for the power supply to prevent excessive SOHP of the HESS.

III. Description of Mathematical Modeling

A. Mathematical Modeling of Electrolytic Cell Stack and Simulink Model

AEs primarily include electrochemical and empirical models. To facilitate analysis of the operating characteristics of the hydrogen production process, an electrochemical model has been used in this paper. The electrolytic cell is considered as a pressure-sensitive nonlinear DC load in the circuit. Within its working range, the output voltage of the electrolytic cell increases with the input current. Therefore, the hydrogen production flow rate (i.e., hydrogen production volume) of the electrolytic cell can be adjusted by adjusting the input current [23]-[25]. The modeling of the electrolyzer must consider the relationship between the power consumption of the stack and flow rate of hydrogen production. These related parameters are obtained from the datasheet and *U-I* characteristic curve provided by the manufacturer. In practical engineering, electrolytic systems consist mainly of several electrolytic cell units connected in series. Therefore, this paper only discusses the modeling of a single electrolytic cell unit. The input and output of the model are the current and hydrogen production flow rate (mol/s), respectively. A simplified circuit diagram of the electrolytic cell unit is shown in Fig. 2, where η_{ohm} is the ohm overvoltage; and η_{act} is the activation overvoltage loss caused by the oxidation reduction reaction in the fuel cells.

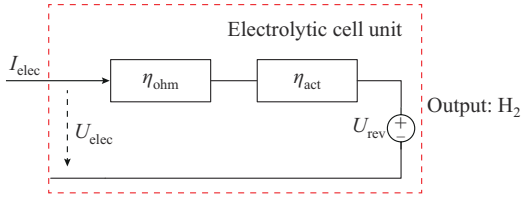

Fig. 2. Simplified circuit diagram of electrolytic cell unit.

According to the *U-I* characteristic curve of the alkaline water electrolytic (AWE) cell obtained from the manufacturer, combined with Faraday's law, a typical electrochemical mathematical model of the electrolytic cell unit can be obtained, as shown in (1)-(3) [7], [9].

$$U_{elec}=U_{rev}+\frac{r_1+r_2T_{elec}}{A_{elec}}I_{elec}+s\left(\frac{t_1+t_2/T_{elec}+t_3/T_{elec}^2}{A_{elec}}I_{elec}+1\right) \tag{1}$$

$$\begin{cases} W_{elec}=\eta_F\dfrac{N_c}{2F}I_{elec} \\ \eta_F=\dfrac{f_2(I_{elec}/A_{elec})^2}{f_1+(I_{elec}/A_{elec})^2} \end{cases} \tag{2}$$

$$U_{rev}=\frac{\Delta G_{elec}}{zF} \tag{3}$$

where U_{elec} is the electrolyzer stack voltage; I_{elec} is the inductor current; U_{rev} is the reversible voltage of the electrolyzer cell under standard conditions; r_1 and r_2 are the Ohmic resistance parameters of the AWE; s, t_1, t_2, and t_3 are the electrode overvoltage coefficients; T_{elec} is the electrolyzer temperature; A_{elec} is the electrolyzer surface area; W_{elec} is the hydrogen production flow rate; N_c is the number of electrolyzer cells; η_F is the Faraday efficiency related to current density; f_1 and f_2 are the Faraday efficiency parameters; ΔG_{elec} is the Gibbs free-energy change of the battery reaction in the standard state (for the chemical reaction that produces water, $\Delta G_{elec}=-474.4$ kJ/mol); z is the number of electrons transferred per reaction ($z=2$); and F is the Faraday's constant ($F=96500$ C/mol).

In the AE model, the form of (1) is similar to the mathematical model form of a hydrogen fuel cell. According to the above mathematical model, the AE model has been built in Simulink, as shown in Appendix A Fig. A1. Its inputs are the electrolytic cell temperature T_{elec} and I_{elec}, and the outputs are W_{elec}, U_{elec}, and η_F.

B. Mathematical Modeling of HESS and Simulink Model

A simplified schematic of the HESS is shown in Fig. 3, consisting of two parts, namely a compressor and a hydrogen starage tank. The hydrogen produced by the electrolyzer is injected into a high-pressure gaseous hydrogen storage tank through a compressor [25], [26]. To model the compressor, the relationship between the inlet hydrogen flow rate, outlet flow rate, outlet and inlet pressure ratio, and electrical energy consumed by the compressor must be considered. The power consumed by the compressor P_{TP} is expressed by (4).

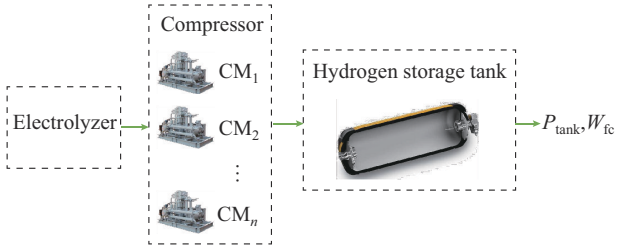

Fig. 3. Simplified schematic of HESS.

$$P_{TP}=W_{elec}C_{pH_2}\frac{T_{TP}}{\eta_{TP}}\left[\left(\frac{P_{outlet}}{P_{inlet}}\right)^{\frac{\gamma-1}{\gamma}}-1\right] \tag{4}$$

where W_{elec} is the hydrogen flow rate at the compressor inlet; C_{pH_2} is the specific heat capacity of hydrogen at a constant pressure; T_{TP} is the compressor inlet temperature; η_{TP} is the compressor operating efficiency; P_{outlet}/P_{inlet} is the ratio of compressor outlet to inlet pressures; and γ is the specific heat ratio of hydrogen under standard conditions.

According to the gas-state equation, the internal pressure of a hydrogen tank is calculated as [27], [28]:

$$P_{tank}=\frac{n_{H_2}RT_{tank}}{V_{tank}} \tag{5}$$

$$n_{H_2}(t_0+\Delta t)=n_0(t_0)+\int_{t_0}^{t_0+\Delta t}q_{H_2}\mathrm{d}t \tag{6}$$

$$q_{H_2}=W_{elec}-W_{fc} \tag{7}$$

where P_{tank} is the pressure inside the tank; n_{H_2} is the amount of substance inside gas tank; V_{tank} is the volume of gas tank; R is the molar gas constant; T_{tank} is the gas temperature;

$n_0(t_0)$ is the initial value of the amount of substance inside the gas tank at time t_0; q_{H_2} is the net hydrogen feed flow rate; and W_{fc} is the hydrogen flow rate at gas tank outlet.

The above mathematical model is based on ideal assumptions as follows.

1) The gas is ideal.

2) The volume of the hydrogen storage tank is constant regardless of the slight change in the volume of the storage tank.

3) The gas temperature is constant.

According to the above mathematical model, a HESS simulation model was built in Simulink, as shown in Appendix A Fig. A2. The system integrates a compressor and hydrogen storage tank to form an integrated hydrogen storage model. Its inputs are the compressor's constant operating temperature, T_{tank}, W_{elec}, and three flags. The three flags can be used to determine whether there are hydrogen input and outflow as well as whether separate hydrogen sales operations are carried out to consider calculation of the economic benefits of independent hydrogen sales involved in the hydrogen storage link. The outputs of the system are the compressor power consumption P_{TP}, current pressure of the storage tank P_{tank} (which indicates the current state of the hydrogen reserve, similar to the SOC of the BESS; we term this the state of hydrogen reserve (SOHR)), and W_{fc}.

C. Mathematical Modeling of PEMFC Stack and Simulink Model

The modeling of the proton-exchange membrane hydrogen fuel cell is based on the PEMFC equivalent circuit structure, as shown in Fig. 4. In this model, the fuel cell is composed of a controlled voltage source connected in series with an equivalent circuit and other basic circuit elements [11], [29].

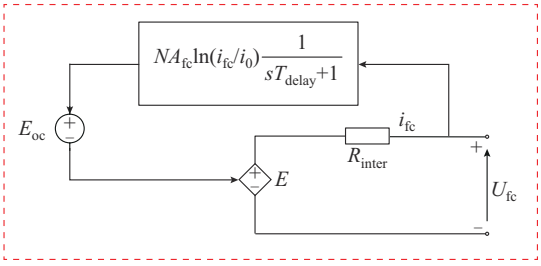

Fig. 4. PEMFC equivalent circuit structure.

where R_{inter} is the internal resistance of fuel cell; and E is the real output voltage of PEMFC. As observed from Fig. 4, the hydrogen fuel cell is internally composed of ohmic and activation overpotentials. These losses are equivalent in the circuit to the RC circuit and are represented by a first-order transfer function in the mathematical model. Considering these losses, the actual output voltage of the hydrogen fuel cell is lower than the open-circuit voltage. Therefore, the actual output voltage of the PEMFC is calculated using (8).

$$\begin{cases} U_{fc} = E_{oc} - \eta_{act} - \eta_{ohm} \\ \eta_{act} = NA_{fc}\ln(i_{fc}/i_0)\dfrac{1}{sT_{delay}+1} \\ \eta_{ohm} = R_{ohm} i_{fc} \end{cases} \tag{8}$$

where U_{fc} is the fuel-cell output voltage; E_{oc} is the open-circuit voltage; η_{act} is the activation overpotential; η_{ohm} is the Ohmic overpotential; N is the number of cells; A_{fc} is the Tafel slope; i_{fc} is the fuel-cell output current; i_0 is the exchange current; T_{delay} is the response time; and R_{ohm} is the fuel-cell stack internal resistance.

In (8), the open-circuit voltage E_{oc}, exchange current i_0, and Tafel slope A_{fc} are calculated using (9)-(11), respectively.

$$E_{oc} = K_c E_{nernst} \tag{9}$$

$$i_0 = \frac{zFk(P_{H_2}+P_{O_2})}{Rh} e^{-\frac{\Delta G}{RT_{fc}}} \tag{10}$$

$$A_{fc} = \frac{RT_{fc}}{z\alpha F} \tag{11}$$

where K_c is the voltage constant under nominal operating conditions; E_{nernst} is the Nernst voltage; z is the number of transferred electrons ($z=2$); α is the charging transfer coefficient; P_{H_2} is the operating pressure of hydrogen; P_{O_2} is the operating pressure of oxygen; ΔG is the change in Gibbs free energy; T_{fc} is the PEMFC operating temperature; k is the Boltzmann constant; and h is the Planck's constant.

The intermediate variables required in (9) and (10) (i.e., hydrogen utilization rate $U_{f_{H_2}}$, oxygen utilization rate $U_{f_{O_2}}$) are determined by:

$$U_{f_{H_2}} = \frac{60000RT_{fc}i_{fc}}{zFP_{fuel}V_{fuel}x} \tag{12}$$

$$U_{f_{O_2}} = \frac{60000RT_{fc}i_{fc}}{2zFP_{air}V_{air}y} \tag{13}$$

where P_{fuel} is the absolute supply pressure of fuel; V_{fuel} is the fuel flow rate; x is the percentage of hydrogen in fuel; P_{air} is the absolute supply pressure of air; V_{air} is the airflow rate; and y is the percentage of oxygen in the oxidant.

P_{H_2}, P_{O_2}, P_{H_2O}, and Nernst voltage E_{nernst} inside the hydrogen fuel-cell stack are defined by (14)-(17), respectively.

$$P_{H_2} = (1 - U_{f_{H_2}})xP_{fuel} \tag{14}$$

$$P_{O_2} = (1 - U_{f_{O_2}})yP_{air} \tag{15}$$

$$P_{H_2O} = (w + 2yU_{f_{O_2}})P_{air} \tag{16}$$

$$\begin{cases} E_{nernst} = 1.2297 + (T_{fc} - 298.15)\dfrac{\Delta S_0}{2F} + \dfrac{RT_{fc}}{2F}\ln(P_{H_2}P_{O_2}^{1/2}) \\ \qquad\qquad T_{fc} < 373\ \text{K} \\ E_{nernst} = 1.2297 + (T_{fc} - 298.15)\dfrac{\Delta S_0}{2F} + \dfrac{RT_{fc}}{2F}\ln\left(\dfrac{P_{H_2}P_{O_2}^{1/2}}{P_{H_2O}}\right) \\ \qquad\qquad T_{fc} \geq 373\ \text{K} \end{cases} \tag{17}$$

where $\Delta S_0 = -44.43$; P_{H_2O} is the partial pressure of water vapor; and w is the percentage of water vapor in the oxidant.

The other parameters required in the model are calculated based on the typical polarization curve data of the fuel-cell stack under standard conditions, and the nominal data are obtained from the datasheet provided by the manufacturer. The parameter calculation formulas are shown in (18)-(20).

$$\begin{cases} \alpha = \dfrac{N \cdot RT_{\mathrm{fc,nom}}}{zF \cdot NA_{\mathrm{fc}}} \\ NA_{\mathrm{fc}} = \dfrac{(V_1 - V_{\mathrm{nom}})(I_{\max} - 1) - (V_1 - V_{\min})(I_{\mathrm{nom}} - 1)}{\ln(I_{\mathrm{nom}})(I_{\max} - 1) - \ln(I_{\max})(I_{\mathrm{nom}} - 1)} \end{cases} \tag{18}$$

where $T_{\mathrm{fc,nom}}$ is nominal operating temperature; V_{nom} and I_{nom} are the voltage and current at nominal operating point, respectively; and $I_{\max}$ and $V_{\min}$ are the current and voltage at the maximum operating point, respectively.

The Gibbs free-energy change is calculated by:

$$\begin{cases} \Delta G = -RT_{\mathrm{fc,nom}} \ln(i_0 / K_1) \\ R_{\mathrm{ohm}} = \dfrac{V_1 - V_{\mathrm{nom}} - NA\ln(I_{\mathrm{nom}})}{I_{\mathrm{nom}} - 1} \\ i_0 = \mathrm{e}^{\frac{V_1 - E_{\mathrm{oc,nom}} + R_{\mathrm{ohm}}}{NA}} \\ K_1 = \dfrac{zFk(P_{\mathrm{H_2,nom}} + P_{\mathrm{O_2,nom}})}{hR} \\ P_{\mathrm{H_2,nom}} = P_{\mathrm{H_2}}\big|_{x = x_{\mathrm{nom}}, U_{f_{\mathrm{H_2}}} = U_{f_{\mathrm{H_2,nom}}}, P_{\mathrm{fuel}} = P_{\mathrm{fuel,nom}}} \\ P_{\mathrm{O_2,nom}} = P_{\mathrm{O_2}}\big|_{y = y_{\mathrm{nom}}, U_{f_{\mathrm{O_2}}} = U_{f_{\mathrm{O_2,nom}}}, P_{\mathrm{air}} = P_{\mathrm{air,nom}}} \\ U_{f_{\mathrm{H_2,nom}}} = \dfrac{\eta_{\mathrm{nom}} \Delta h^0(\mathrm{H_2O(gas)})N}{zFV_{\mathrm{nom}}} \\ U_{f_{\mathrm{O_2,nom}}} = \dfrac{60000RT_{\mathrm{nom}} \cdot NI_{\mathrm{nom}}}{2z \cdot FP_{\mathrm{air,nom}} V_{\mathrm{air,nom}} y_{\mathrm{nom}}} \end{cases} \tag{19}$$

where $E_{\mathrm{oc,nom}}$ and V_1 are the voltages at 0 and 1 A, respectively; η_{nom} is the nominal lower heating value (LHV) stack efficiency; $V_{\mathrm{air,nom}}$ is the nominal airflow rate; $P_{\mathrm{air,nom}}$ and $P_{\mathrm{fuel,nom}}$ are the absolute supply pressures of air and fuel, respectively; x_{nom} is the nominal composition of hydrogen in fuel; y_{nom} is the nominal composition of oxigen in the air; w_{nom} is the nominal compositions of gaseous water in the oxidant; and H_2O(gas) represents gaseous water.

The nominal voltage constant K_{c} of the PEMFC stack is determined by:

$$\begin{cases} K_{\mathrm{c}} = \dfrac{E_{\mathrm{oc,nom}}}{E_{\mathrm{nernst,nom}}} \\ E_{\mathrm{nernst,nom}} = E_{\mathrm{nernst}}\big|_{U_{f_{\mathrm{H_2}}} = U_{f_{\mathrm{H_2,nom}}}, U_{f_{\mathrm{O_2}}} = U_{f_{\mathrm{O_2,nom}}}, T_{\mathrm{fc}} = T_{\mathrm{fc,nom}}} \end{cases} \tag{20}$$

For the above mathematical model, a corresponding simulation model has been established in Simulink to facilitate subsequent experimental verification, as illustrated in Appendix A Fig. A3. The system inputs are P_{fuel}, fuel flow rate V_{fuel}, P_{air}, air flow rate V_{air}, working temperature T_{fc}, percentage of hydrogen in the fuel x, and percentage of oxygen in the oxidizer y, while the outputs of the system are the PEMFC voltage and measurement signals.

Note that the PEMFC model proposed above is developed using the following assumptions.

1) The gas is ideal.

2) A constant temperature is maintained during the operation of the PEMFC stack.

3) The water vapor content (humidity) inside the PEMFC stack remains constant.

4) The pressure changes of fuel and air in the intake pipe are negligible.

5) The internal resistance of the PEMFC is constant.

IV. Simulation Verification of HESS Model in Wind-PV-HESS-BESS Hybrid System

A. Verification Within MG System

The HESS model proposed herein is integrated into the grid-connected wind-PV-HESS-BESS hybrid system to simulate the accuracy of the proposed model. The Simulink model of the wind-PV-HESS-BESS hybrid system is shown in Appendix A Fig. A4. The nominal power of the PV system in the MG is 20 kW, and the nominal power of the lithium BESS on the AC side is 135 kWh with a 50% initial SOC. The model parameter settings of the HESS (AWE, hydrogen storage tank, and PEMFC) are listed in Tables I-III.

TABLE I
Model Parameters of AWE

Symbol	Value	Unit
r_1	8.05×10^{-5}	$\Omega\cdot m^2$
r_2	-2.5×10^{-7}	$\Omega\cdot m^2\cdot K^{-1}$
t_1	−1.002	$A^{-1}\cdot m^2$
t_2	8.424	$A^{-1}\cdot m^2\cdot K$
t_3	247.3	$A^{-1}\cdot m^2\cdot K^2$
s	0.185	V
A_{elec}	0.25	m^2
ΔG_{elec}	−474.4	kJ/mol
f_1	250	$mA^2\cdot cm^4$
f_2	0.98	
N_{c}	21	
F	96485	C/mol^{-1}

TABLE II
Model Parameters of Hydrogen Storage Tank

Symbol	Value	Unit
$C_{p\mathrm{H_2}}$	14.0500	kJ/(kg·K)
γ	1.4140	
V_{tank}	0.2400	m^3
R	8.3145	$J\cdot mol^{-1}\cdot K^{-1}$

TABLE III
Model Parameters of PEMFC

Symbol	Value	Unit	Symbol	Value	Unit
N	65		x_{nom}	99.5	%
$V_{\min}$	37	V	y_{nom}	21	%
$I_{\max}$	225	A	w_{nom}	1	
V_{nom}	45	V	η_{nom}	55	%
I_{nom}	133.3	A	$T_{\mathrm{fc,nom}}$	338.15	K
$E_{\mathrm{oc,nom}}$	65	V	z	2	
V_1	63	V	k	1.38×10^{-23}	J/K
$V_{\mathrm{air,nom}}$	297	L/min	h	6.626×10^{-34}	J·s
$P_{\mathrm{air,nom}}$	150000	Pa	ΔS_0	21	
$P_{\mathrm{fuel,nom}}$	100000	Pa			

Figure 5 shows the voltage and current waveforms of the AC power grid, DC-side voltage of the PV grid-connected system, and simulation curve of PV power. The grid voltage and frequency are 380 V and 50 Hz, respectively. The irradiance starts increasing gradually at 0.2 s, so the corresponding PV power increases and stabilizes at 0.5 s; the voltage of the DC-side busbar of the PV power generation module stabilizes at 700 V. In Fig. 5(d), the irradiance of the PV starts increasing at point 1 and stabilizes at point 2.

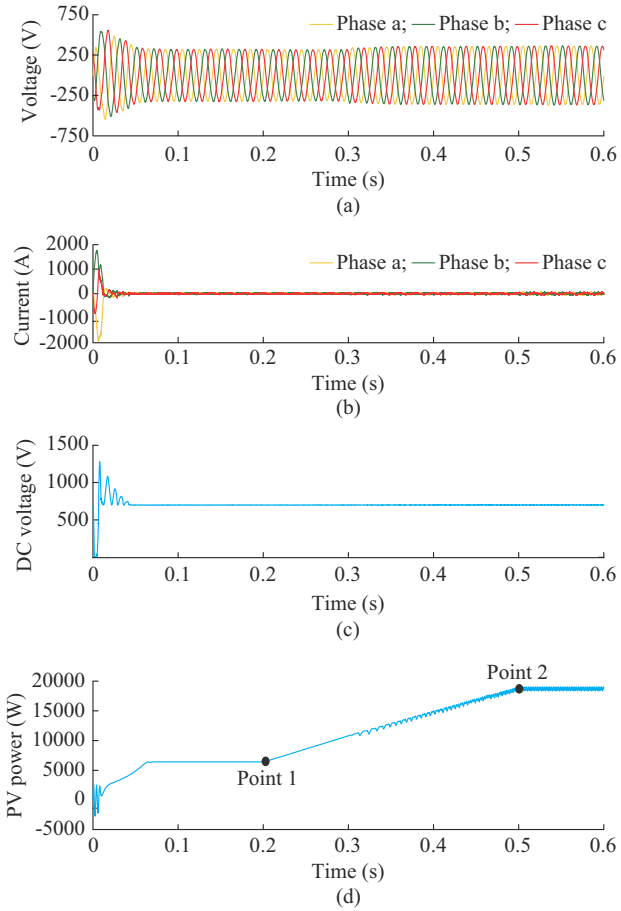

Fig. 5. Voltage and current waveforms of AC power grid, DC-side voltage of PV grid-connected system, and simulation curve of PV power. (a) Grid voltage. (b) Grid current. (c) DC-side voltage of PV grid-connected system. (d) PV power.

Figure 6 shows the SOC variation curve of the lithium BESS in the MG. We set the initial SOC of the BESS to be 50%; when it is higher than 50%, it means that there is surplus renewable energy power in the MG, which is then used to charge the energy storage system while ensuring hydrogen production. When the SOC is below 50%, the power supply in the MG is deemed insufficient, and the BESS power needs to be consumed to compensate for the power and hydrogen demands.

Figure 7 shows the operating characteristics of the HESS. The electrolyzer consumes electricity from the three-phase AC bus for electrolysis of water. The hydrogen production flow rate stabilizes at 5 kg/s. As the amount of hydrogen increases, the power consumption of the compressor also increases. The pressure inside the hydrogen storage tank also increases, which conforms to the operation of the actual physical system, thereby verifying the correctness of the proposed model.

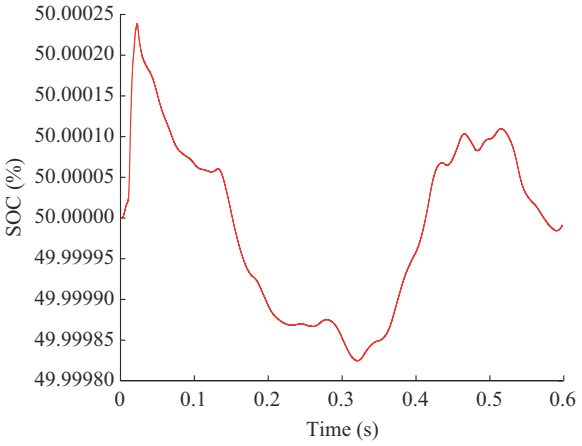

Fig. 6. SOC variation curve of lithium BESS in MG.

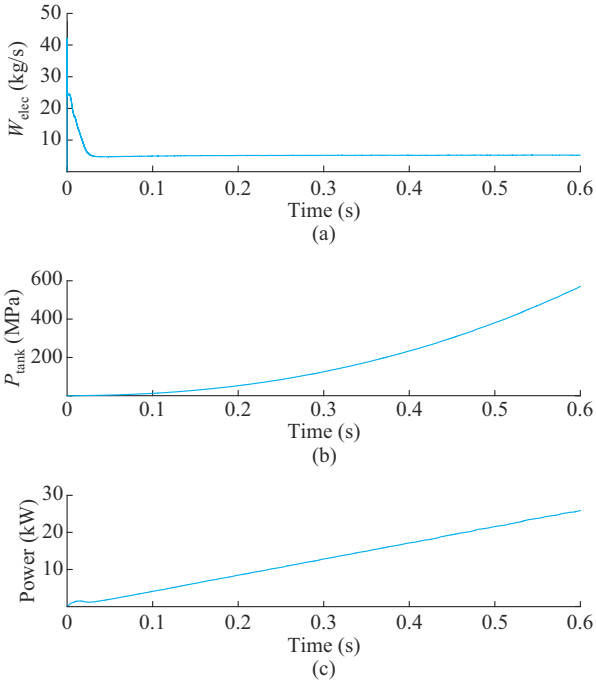

Fig. 7. Operating characteristics of HESS. (a) Hydrogen flow rate. (b) Pressure of hydrogen storage tank. (c) Power consumption of compressor.

In addition, when hydrogen is sold to a refueling station, we consider its impact on the operating characteristics of the HESS. In this paper, the working conditions are set as follows.

1) Case 1: at 0-0.2 s, the alkaline electrolyzer in the HESS produces hydrogen, and the sale of hydrogen is not considered. In this case, the HESS operates in the hydrogen production and energy storage modes. The distributed energy and auxiliary energy storage unit in the MG supplies power to the HESS to produce hydrogen, and the PV and wind turbines obtain the maximum power from the power supply at

the maximum power point.

2) Case 2: at 0.2-0.6 s, the HESS stops hydrogen production by electrolysis of water, starts the proton-exchange membrane hydrogen fuel cells, and sells hydrogen simultaneously. In this case, the SOHR change of the HESS is affected by two factors, namely fuel-cell power generation and hydrogen market transaction. These two hydrogen distribution paths will bring economic benefits to the MG by connecting to the electricity and chemical markets, respectively, which has significance for the construction of practical projects. The characteristic variation curves of the HESS-related parameters are shown in Fig. 8.

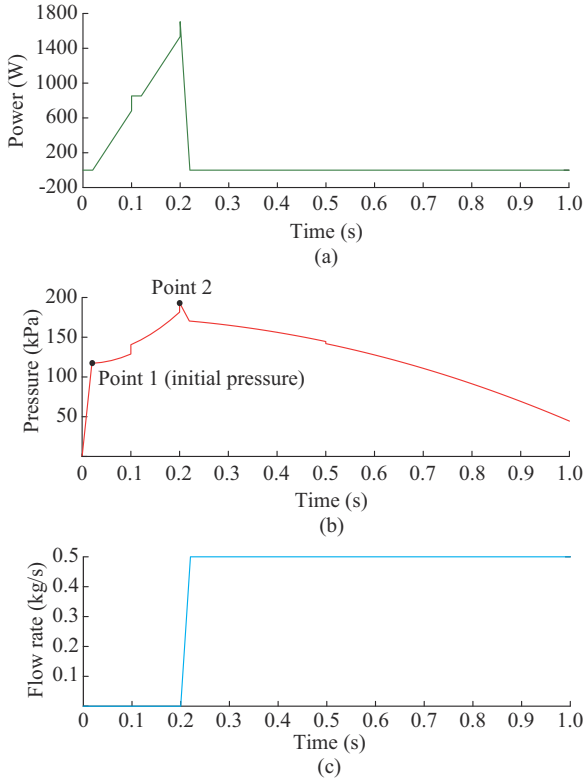

Fig. 8. Characteristic variation curves of HESS-related parameters. (a) Power consumption of compressor. (b) Pressure of hydrogen storage tank. (c) Flow rate of fuel cell hydrogen.

As shown in Fig. 8, the electrolyzer continues to produce hydrogen before 0.2 s, and the power consumption of the compressor increases with hydrogen production. Starting from 0.2 s, the hydrogen storage tank supplies hydrogen to the proton-exchange membrane hydrogen fuel cell, and the hydrogen flows into the hydrogen fuel cell at a flow rate of 0.5 kg/s to commence power generation. In addition, we believe that hydrogen exists in the initial state of the hydrogen storage tank; therefore, the initial pressure of the hydrogen storage tank is not zero. As shown in Fig. 8, the power consumption and tank pressure of the compressor increase before 0.2 s. At 0.2 s, the pressure of the hydrogen storage tank drops suddenly; this is because the system operation mode changes from case 1 to case 2 at 0.2 s, i.e., only the operation of selling hydrogen is carried out, resulting in rapid declines in the hydrogen storage capacity and pressure of the storage tank.

B. Analysis of Operating Characteristics of Hydrogen Fuel Cell

In addition to the above-mentioned data analyses and verifications, this paper focuses on analysis of the operating characteristic curve of the hydrogen fuel cell. The simulation model considers the transients caused by manifold filling dynamics, membrane water content, supercharging device, air compressor adjustment, etc. Ignoring the temperature changes during the rapid change processes, the operating characteristic curves of hydrogen fuel cell are shown in Fig. 9.

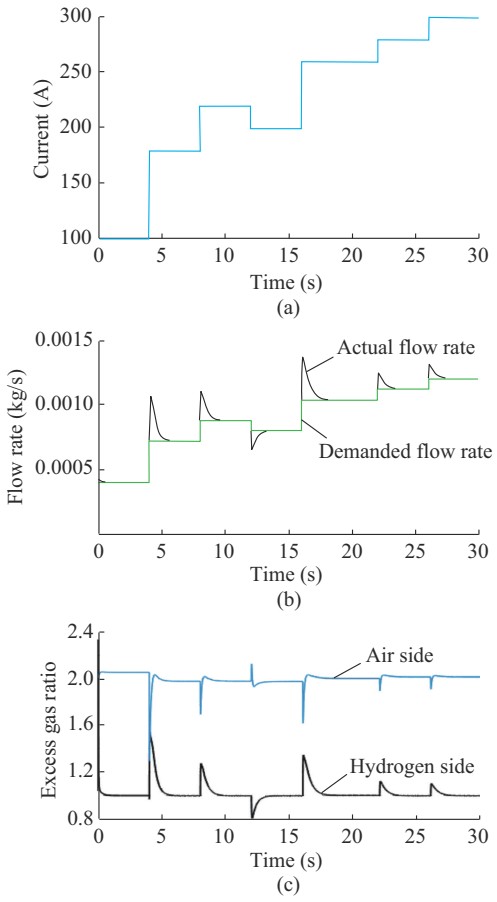

Fig. 9. Operating characteristic curves of hydrogen fuel cell. (a) Hydrogen demand curve. (b) Hydrogen inlet flow rate. (c) Excess gas ratio.

Considering the actual hydrogen demand change, the curve is a series of step changes, as shown in Fig. 9(a). The anode intake flow rate follows the trend of the demand current curve and differs from the fluctuations of the demand inlet flow rate at the moment of the step change in the demand current. This flow fluctuation reflects the delay characteristics caused by the adjustment of the anode pressure. The cathode inlet flow rate also exhibits a certain degree of fluctuation, which is related to the dynamic characteristics of the air compressor and air-supply pipeline. It is more intuitive to observe the changes in the excess coefficient curve. At the moment of a sudden load change, the change in air supply is

affected by the adjustment characteristics of the air compressor, and the dynamic characteristics of the air-supply pipeline lag behind the changes in the stack demand. This hysteresis is also the reason for setting the excess coefficient on the air side because when the supply is not excessive. For a sudden change in the load current, the fuel-cell stack may suffer from oxygen starvation, resulting in a decline of the battery output voltage, flooding of the stack, and even damage to the fuel and service life of battery. In Fig. 9(c), it is observed that although the cathode excess coefficient lags behind the change in demand, it remains greater than 1.

V. Conclusion

An HESS is an indispensable part for constructing a new power system with renewable energy as the main source. Its design and simulations require a simple and realistic model, which is necessary for determining the capacity of the HESS. In this paper, an integrated modeling method is proposed for HESSs, and a HESS model including AEs, ideal air compressors, high-pressure hydrogen storage tanks, PEMFCs, and other MG components is developed in Simulink. The alkaline water electrolysis system is a stack composed of 0.25 m^2 electrodes and 210 cells. The hydrogen storage model involves a hydrogen storage tank of capacity 240 L and an ideal air compressor with a rated efficiency of 85%. The fuel cell consists of 65 cells, and its rated power is 6 kW. The HESS model parameters can be modified to simulate similar systems with different hydrogen production capabilities, storage capacities, and power generation abilities. The grid-connected operational characteristic curves of the HESS in the hybrid Wind-PV-HESS-BESS system are obtained, including the current and voltage waveforms, efficiency curves, and power consumption curves. Therefore, the power consumption of each subsystem in the HESS can be estimated, and the operating parameters can be determined with good scalability. In the final MG verification, we demonstrate how the HESS model could be used with other renewable energy systems and as a perfect starting point for the design and simulation of a comprehensive hydrogen energy utilization system.

Appendix A

Figures A1-A4 present the Simulink models used in the paper.

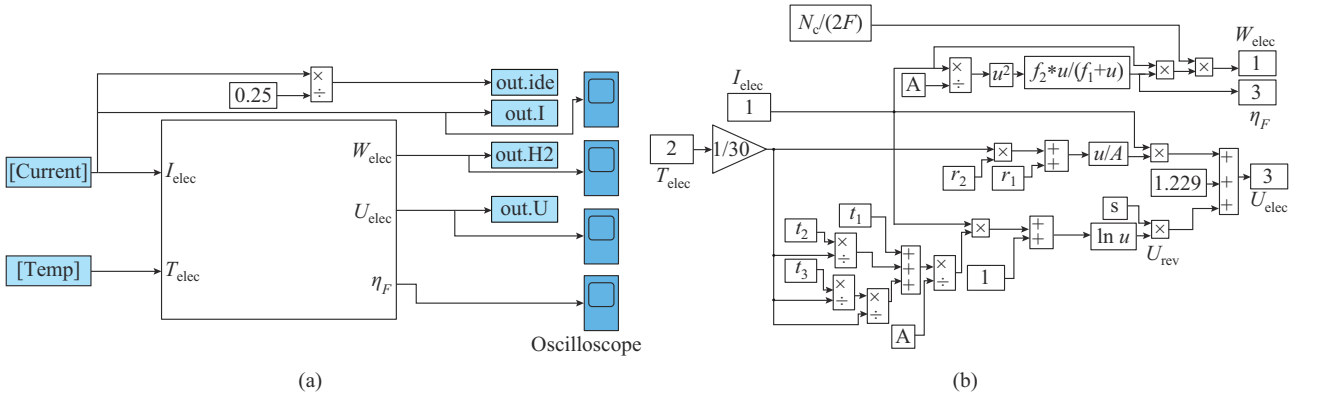

Fig. A1. Simulink model of AE. (a) Overall simulation diagram of electrolyzer. (b) Simulation diagram of internal mathematical model of electrolyzer system.

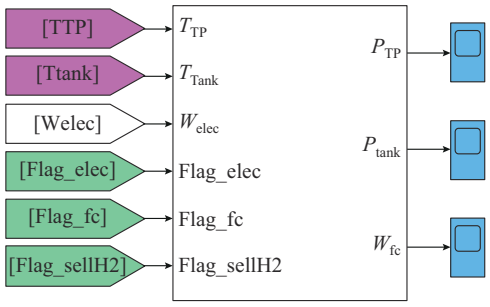

Fig. A2. Simulink model of HESS.

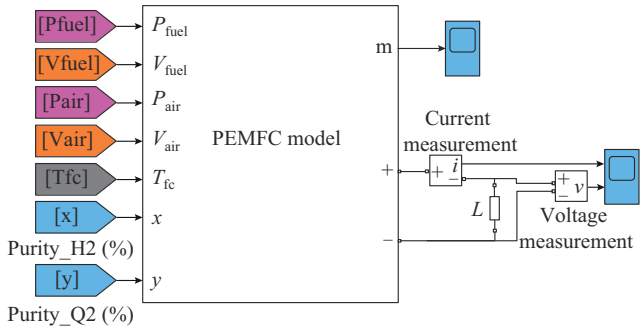

Fig. A3. Simulink model of PEMFC.

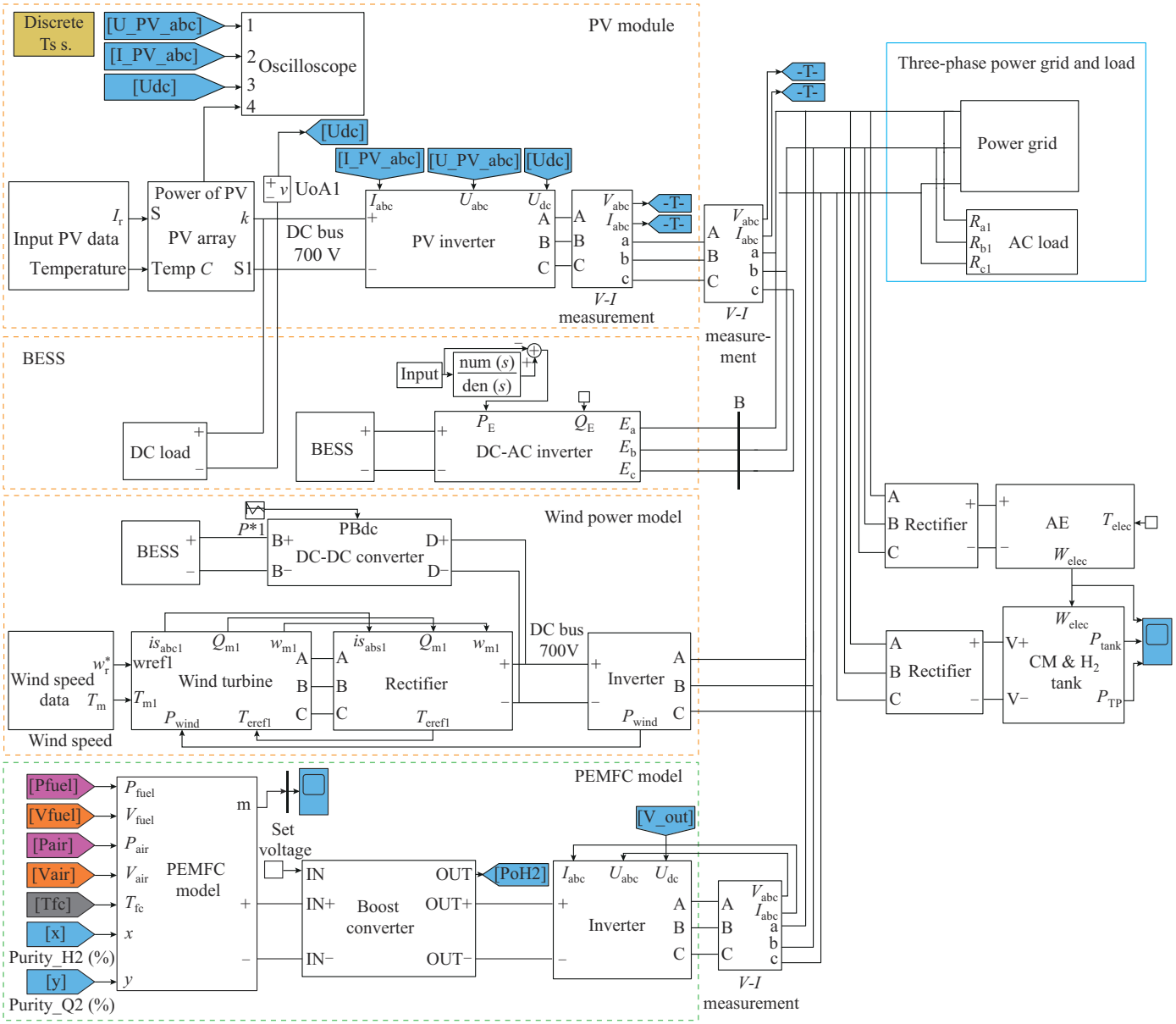

Fig. A4. Simulink model of wind-PV-HESS-BESS hybrid systems.

REFERENCES

[1] J. Li, G. Li, S. Ma *et al*., "Overview of the progress and development prospects of key technologies for hydrogen production under the goal of carbon neutrality," *Thermal Power Generation*, vol. 50, no. 6, pp. 1-8, Feb. 2021.

[2] J. Li, G. Li, S. Ma *et al*., "An overview on hydrogen energy storage and transportation technology and its typical application in power system," *Modern Electric Power*, vol. 38, no. 5, pp. 535-545, Apr. 2021.

[3] S. You, J. Hu, Y. Zong *et al*., "Value assessment of hydrogen-based electrical energy storage in view of electricity spot market," *Journal of Modern Power Systems and Clean Energy*, vol. 4, no. 4, pp. 626-635, Oct. 2016.

[4] L. Kong, G. Cai, L. Li *et al*., "Online energy control strategy and experimental platform of integrated energy system of wind, photovoltaic and hydrogen," *Transactions of China Electrotechnical Society*, vol. 33, no. 14, pp. 3371-3384, Jun. 2018.

[5] G. Cai, C. Chen, L. Kong *et al*., "Modeling and control of grid-connected system of wind/PV/electrolyzer and SC," *Power System Technology*, vol. 40, no. 10, pp. 2982-2990, May 2016.

[6] Y. Wang, G. Yang, J. Zhuang *et al*., "Zero-error frequency regulation control method for microgrids based on consensus algorithm," *Electric Power*, vol. 53, no. 10, pp. 187-191, Feb. 2020.

[7] Y. Chen and L. Zhou, "Modeling and control of hybrid PV-supercapacitor-hydrogen system," *Modern Electric Power*, vol. 34, no. 3, pp. 88-94, Dec. 2016.

[8] Z. Shao, J. Wu, Q. Zhao *et al*., "Cost effectiveness analysis model for wind power produce hydrogen system and simulation," *Technology Economics*, vol. 37, no. 6, pp. 69-75, Jun. 2018.

[9] I. Abadlia, L. Hassaine, A. Beddar *et al*., "Adaptive fuzzy control with an optimization by using genetic algorithms for grid connected a hybrid photovoltaic-hydrogen generation system," *International Journal of Hydrogen Energy*, vol. 45, no. 43, pp. 22589-22599, Jun. 2020.

[10] S. N. M. O. Tremblay and L. A. Dessaint, "A generic fuel cell model for the simulation of fuel cell vehicles," in *Proceedings of 2009 IEEE Vehicle Power and Propulsion Conference*, Dearborn, USA, Sept. 2009, pp. 1722-1729.

[11] K. J. Runtz and M. D. Lyster, "Fuel cell equivalent circuit models for passive mode testing and dynamic mode design," in *Proceedings of Canadian Conference on Electrical and Computer Engineering*, Saskatoon, Canada, May 2005, pp. 794-797.

[12] T. Yigit and O. Selamet, "Mathematical modeling and dynamic simulink simulation of high-pressure PEM electrolyzer system," *International Journal of Hydrogen Energy*, vol. 41, no. 32, pp. 13901-13914, Jun. 2016.

[13] M. Alam, K. Kumar, S. Verma *et al*., "Renewable sources based DC

microgrid using hydrogen energy storage: modelling and experimental analysis," *Sustainable Energy Technologies and Assessments*, vol. 46, no. 2, p. 100840, May 2020.
[14] G. Matute, J. M. Yusta, J. Beyza *et al.*, "Multi-state techno-economic model for optimal dispatch of grid connected hydrogen electrolysis systems operating under dynamic conditions," *International Journal of Hydrogen Energy*, vol. 46, no. 2, pp. 1449-1460, Oct. 2020.
[15] F. Alshehri, V. G. Suarez, J. L. R. Torres *et al*., "Modelling and evaluation of PEM hydrogen technologies for frequency ancillary services in future multi-energy sustainable power systems," *Heliyon*, vol. 5, no. 4, p. 1396, Apr. 2019.
[16] P. Kong, Z. Jiang, L. Yang *et al*., "Mechanism and risk quantification model design of hydrogen storage system participation in power market," *Distribution & Utilization*, vol. 39, no. 1, pp. 31-39, Jan. 2022.
[17] N. Yang, T. Yuan, Y. Zhang *et al.*, "Layout optimization of pre-manufactured hydrogen energy storage power station based on surrogate method," *Transactions of China Electrotechnical Society*, vol. 36, no. 3, pp. 473-485, May 2021.
[18] Y. Jiang and X. Shen, "Construction and application of digital twin in hydrogen production system of alkaline water electrolyzer," *High Voltage Engineering*, vol. 48, no. 5, pp. 1673-1683, Feb. 2022.
[19] L. Stoyanov, "Modeling of hybrid system with photovoltaic panels-fuel cells generation and hydrogen storage using electrolyzer," in *Proceedings of 2021 17th Conference on Electrical Machines, Drives and Power Systems (ELMA)*, Sofia, Bulgaria, Jul. 2021, pp. 1-4.
[20] S. S. Khan, H. Shareef, and A. A. Ibrahim, "Improved semi-empirical model of proton exchange membrane fuel cell incorporating fault diagnostic feature," *Journal of Modern Power Systems and Clean Energy*, vol. 9, no. 6, pp. 1566-1573, Nov. 2021.
[21] A. Halme, J. Selkinaho, T. Noponen *et al*., "An alternative concept for DMFC-combined electrolyzer and H_2 PEMFC," *International Journal of Hydrogen Energy*, vol. 41, no. 4, pp. 2154-2164, Jan. 2016.
[22] F. J. Vivas, A. Heras, F. Segura *et al*., "A review of energy management strategies for renewable hybrid energy systems with hydrogen backup," *Renewable & Sustainable Energy Reviews*, vol. 82, no. 1, pp. 126-155, Feb. 2018.
[23] W. Yin, L. Liu, and X. Rui, "Modeling and operation performance analysis of hybrid drive wind power generation system with hydrogen energy storage," *Electric Power Automation Equipment*, vol. 40, no. 10, pp. 64-70. Oct. 2020.
[24] K. Wang, Z. Zhao, and J. Luo, "Simulation and performance analysis of hydrogen storage system for wind solar complementary power generation," *Energy Conservation*, vol. 38, no. 11, pp. 79-84. Nov. 2019.
[25] L. Kong, G. Cai, and S. Xue, "Modeling and coordinated control strategy of large scale grid-connected wind/photovoltaic/energy storage hybrid energy conversion system," *Mathematical Problems in Engineering*, vol. 2015, no. 1, pp. 1-14, Jan. 2015.
[26] G. Cai and L. Kong, "Techno-economic analysis of wind curtailment/hydrogen production/fuel cell vehicle system with high wind penetration in China," *CSEE Journal of Power and Energy Systems*, vol. 3, no. 1, pp. 44-52, Mar. 2017.
[27] A. G. Khayrullina, D. Blinov, and V. Borzenko, "Novel kW scale hydrogen energy storage system utilizing fuel cell exhaust air for hydrogen desorption process from metal hydride reactor," *Energy*, vol. 183, no. 15, pp. 1244-1252, Sept. 2019.
[28] J. Romdhane, H. Louahlia, and M. Marion, "Dynamic modeling of an eco-neighborhood integrated micro-CHP based on PEMFC: performance and economic analyses," *Energy & Buildings*, vol. 166, no. 17, pp. 93-108, Sept. 2018.
[29] J. Hwang, L. Lai, W. Wu *et al*., "Dynamic modeling of a photovoltaic hydrogen fuel cell hybrid system," *Energy*, vol. 34, no. 23, pp. 9531-9542, Oct. 2009.

Jianlin Li received the B. Sc. and M. Sc. degrees in electrical engineering from Taiyuan University of technology, Taiyuan, China, in 1998 and 2001, respectively, and the Ph. D. degree in electrical engineering from Zhejiang University, Hangzhou, China, in 2005. He is currently working as a Full Professor in North China University of Technology, Beijing, China. His research interests include large-scale energy storage system technology and application, grid connection technology for renewable energy power generation, and modeling and stability analysis of energy storage system.

Guanghui Li received the B.E. degree in electrical engineering from Yangtze University, Jingzhou, China, in 2016. He is currently pursuing the M.Sc. degree in electrical engineering in North China University of Technology, Beijing, China. His research interests include development and application of hydrogen energy system, control solution for integrated energy systems, and power system dynamics.

Suliang Ma received the B.Sc. and M.Sc. degrees in electrical and electronic engineering from China University of Mining and Technology, Xuzhou, China, in 2011 and 2014, respectively, and the Ph.D. degree in electrical engineering from Beihang University, Beijing, China, in 2020. He is currently working as a Research Assistant in the same university. His research interests include reliability analysis of power system, large-scale energy storage technology and safety application, and power system dynamics and control.

Zhonghao Liang received the B. E. degree in electrical engineering from North China University of Water Resources and Electric Power, Zhengzhou, China, in 2013. She is currently pursuing the M.A. degree in electrical engineering in North China University of Technology, Beijing, China. Her research interests include development and application of hydrogen energy system, and control solution for integrated energy systems and power system dynamics.

Yaxin Li received the B. E. degree in electrical engineering from Taiyuan University of technology, Taiyuan, China, in 2018. She is currently pursuing the M.A. degree in electrical engineering in North China University of Technology, Beijing, China. Her research interests include echelon utilization of retired batteries, and control solution for integrated energy systems and power system.

Wei Zeng received the Ph. D. degree in electrical engineering from Wuhan University, Wuhan, China, in 2010. He is currently working as a Senior Engineer in State Grid Jiangxi Electric Power Co., Ltd. Electric Power Research Institute, Nanchang, China. His research interests include renewable energy and energy storage technology, control solution for integrated energy systems, and power system dynamics.